

2

AD-A257 695



Quarterly Technical Report 1 • November 1992

IR MATERIALS PRODUCIBILITY

A. Sher, Program Director
M.A. Berding, Sr. Research Physicist
Physical Electronics Laboratory

A.-B. Chen, Auburn University
M.W. Muller, Consultant

SRI Project 3820

Prepared for:

Contracting Officers Technical Representative
Defense Advanced Research Projects Agency
Microelectronics Technology Office (MTO)
3701 N. Fairfax Drive
Arlington, VA 22203-1714

Attn: Mr. Raymond Balcerak

ARPA Order No. 8557; Program Code Nos. 2H20, 2D10

Contract MDA972-92-C-0053

Covering the period: 12 August through 31 October 1992

The views and conclusions contained in this document are those of the authors and should not be interpreted as representing the official policies, either expressed or implied, of the Defense Advanced Research Projects Agency or the U.S. Government.

Approved for Public Release
Distribution Unlimited

92 11 10 059

92-29639



3387

DTIC
ELECTE
NOV 17 1992
S **D**
C

IR MATERIALS PRODUCIBILITY

A. Sher, Program Director
M.A. Berding, Sr. Research Physicist
Physical Electronics Laboratory

A.-B. Chen, Auburn University
M.W. Muller, Consultant

SRI Project 3820

Prepared for:

Contracting Officers Technical Representative
Defense Advanced Research Projects Agency
Microelectronics Technology Office (MTO)
3701 N. Fairfax Drive
Arlington, VA 22203-1714

Attn: Mr. Raymond Balcerak

Sponsored by:

Defense Advanced Research Projects Agency
Microelectronics Technology Office (MTO)
Infrared Focal Plane Array Program
ARPA Order No. 8557; Program Code Nos. 2H20, 2D10
Issued by DARPA/CMO under Contract MDA972-92-C-0053

Covering the period: 12 August through 31 October 1992

The views and conclusions contained in this document are those of the authors and should not be interpreted as representing the official policies, either expressed or implied, of the Defense Advanced Research Projects Agency or the U.S. Government.

Approved for Public Release
Distribution Unlimited

Approved:

Ivor Brodie, Director
Physical Electronics Laboratory
Computing and Engineering Sciences Division

DTIC QUALITY INSPECTED 4

Accession For	
NTIS GRA&I	<input checked="checked" type="checkbox"/>
DTIC TAB	<input type="checkbox"/>
Unannounced	<input type="checkbox"/>
Justification	
By	
Distribution/	
Availability Codes	
Dist: Special	
A-1	

REPORT DOCUMENTATION PAGE			Form Approved OMB No. 0704-0188	
Public reporting burden for this collection of information is estimated to average 1 hour per response, including the time for reviewing instructions, searching existing data sources, gathering and maintaining the data needed, and completing and reviewing the collection of information. Send comments regarding this burden estimate or any other aspect of this collection of information, including suggestions for reducing this burden, to Washington Headquarters Services, Directorate for Information Operations and Reports, 1215 Jefferson Davis Highway, Suite 1204, Arlington, VA 22202-4302, and to the Office of Management and Budget, Paperwork Reduction Project (0704-0188), Washington, DC 20503.				
1. AGENCY USE ONLY (Leave Blank)	2. REPORT DATE November 1992	3. REPORT TYPE AND DATES COVERED Quarterly Tech. Rpt. 1, 8-12-92 to 10-31-92		
4. TITLE AND SUBTITLE IR Materials Producibility		5. FUNDING NUMBERS		
6. AUTHOR(S) A. Sher, M.A. Berding, SRI International A.-B. Chen, Auburn University; M. Muller, Consultant				
7. PERFORMING ORGANIZATION NAME(S) AND ADDRESS(ES) SRI International 333 Ravenswood Avenue Menlo Park, CA 94025		8. PERFORMING ORGANIZATION REPORT NUMBER		
9. SPONSORING/MONITORING AGENCY NAME(S) AND ADDRESS(ES) Defense Advanced Research Projects Agency Microelectronics Technology Office (MTO) Infrared Focal Plane Array Program 3701 N. Fairfax Drive Arlington, VA 22203-1714		10. SPONSORING/MONITORING AGENCY REPORT NUMBER		
11. SUPPLEMENTARY NOTES				
12a. DISTRIBUTION/AVAILABILITY STATEMENT Approved for public release; distribution unlimited		12b. DISTRIBUTION CODE		
13. ABSTRACT (Maximum 200 words) We have included the gradient correction to the local density approximation, and used it to calculate the cohesive energies for HgTe, CdTe, ZnTe, and ZnSe. We find excellent agreement with experiment. The gradient correction was also added to the defect formation energies in HgTe (used as a model for HgCdTe). Again, the calculated defect densities are in very good agreement with experiment. We have also examined the band structure of HgCdTe and find it to be highly nonparabolic; we have begun to explore the consequences on the defect densities and other device properties. We have examined the properties of dislocations in HgCdTe and conclude that the trapping of carriers at localized states at the dislocation core is not responsible for the observed effects of dislocations on devices. We are currently examining the effect of dislocation-related strain fields on the piezoelectric HgCdTe, and their consequences on device properties. We have begun to calculate the defect formation energies in ZnSe, including relaxation of the nearest neighbors.				
14. SUBJECT TERMS native point defects; defect densities; photonic materials; IRFPAs; dislocations; HgTe; CdTe; ZnSe; HgCdTe			15. NUMBER OF PAGES 29	16. PRICE CODE
17. SECURITY CLASSIFICATION OF REPORT Unclassified	18. SECURITY CLASSIFICATION OF THIS PAGE Unclassified	19. SECURITY CLASSIFICATION OF ABSTRACT Unclassified	20. LIMITATION OF ABSTRACT None	

SUMMARY

The work summarized in this report covers the first quarter of a program with a goal that is twofold: first, to study the properties of native point and line defects in IRFPA active and substrate materials, and second, to study the properties of native point defects in two classes of photonic materials, the wide-gap II-VI compound (ZnSe as the prototype for which impurity properties will also be calculated) and the nonlinear optical materials (LiNbO₃ as the prototype). Our accomplishments in the first quarter include:

- Preliminary determination of the concentration of native point defects in Hg_{0.8}Cd_{0.2}Te as a function of anneal temperature and mercury pressure.
- Identification of mechanisms likely to account for effects of dislocations on IRFPA performance, and initial quantitative analysis.
- Identification of features of the band structure important to native point defect determination and also important to transport and lifetime analyses.
- Initial calculation of the properties of ZnSe, including new gradient correction terms.

CONTENTS

1.	INTRODUCTION	1
2.	NATIVE POINT DEFECTS IN IRFPA ACTIVE AND SUBSTRATE MATERIALS	1
2.1	Native Point Defects in $\text{Hg}_{0.8}\text{Cd}_{0.2}\text{Te}$	1
2.2	Dislocations in HgCdTe	2
3.	PHOTONIC MATERIALS	3
4.	WORK PLANNED	3
	REFERENCES	4
	APPENDICES	
A	$\text{Hg}_{0.8}\text{Cd}_{0.2}\text{Te}$ Native Defects: Densities and Dopant Properties	A-1
B	Dislocation Space Charge	B-1
C	Piezoelectric Field of a Straight Dislocation	C-1

1. INTRODUCTION

We have added a number of improvements to our calculation of the native defect formation energies; these improvements will apply to HgCdTe, ZnSe, and LiNbO₃. First, we have included a gradient correction to the local density approximation that impacts the manner in which the exchange-correlation energy is calculated. This represents a significant correction to energies in which atoms are exchanged between the solid and free-atoms state; for example, with this correction the cohesive energies of the II-VI compounds are predicted in excellent agreement with experiment (< 5%).

We have also begun to calculate the full nonradial relaxation of the defects; because relaxations may be large, some interatomic distances increase, while others decrease. This has necessitated careful examination of parameters used in the codes, such as the size of the basis set. We are completing this analysis and have begun to calculate relaxation energies.

Finally, we have developed an approach that has permitted us to identify the primary ionization state(s) of defects. Although the local density approximation, upon which our methods are based, predicts band gaps that are too small in the semiconductors, this approach appears to yield reasonable agreement with the available experiments for the prototypical defect we have studied. Later in the program, we will be making improvements to this portion of our calculations.

2. NATIVE POINT DEFECTS IN IRFPA ACTIVE AND SUBSTRATE MATERIALS

2.1 NATIVE POINT DEFECTS IN Hg_{0.8}Cd_{0.2}Te

We have included the gradient correction in the native defect formation energies for HgTe, and calculated the resulting defect densities in Hg_{0.8}Cd_{0.2}Te as a function of temperature and mercury pressure. The ionization states of the defects have also been included in our analysis. We find good agreement with the available experimental data.

We confirm the mercury vacancy as the dominant defect in narrow-gap HgCdTe. We predict that the tellurium antisite will be an important secondary defect, and are currently investigating if it is the "residual donor" in annealed HgCdTe. The results of our work were presented at the 1992 *U.S. Workshop on the Physics and Chemistry of Mercury Cadmium Telluride and Other IR Materials*, held in Boston on 13 through 15 October. A copy of the paper presented at that meeting is presented in Appendix A.

Because HgCdTe is grown and processed at temperatures at which the material is intrinsic and degenerate, and because the defects are ionized, too, and interact with the electron-hole gas, we must know the intrinsic reaction constant in order to calculate the concentration of ionized defects. While there has been much study of the band edge properties of HgCdTe at low temperatures, the relevant properties, (band-gap E_g , and electron and hole effective masses) at the elevated temperatures have not been studied. In the paper in Appendix A, we used expressions for E_g from the literature, and extrapolated them to the high temperatures; temperature independence of the shape of the conduction and valence bands was assumed. Such an extrapolation must be replaced by better experimental results or further theory. In addition, we have found that the Moss-Bornstein shift is large at the higher temperatures (of the order of several tenths of an eV), and needs to be corrected for in the absorption results in the literature.

Furthermore, we have found from our theoretical calculations that the electron band shape is highly nonparabolic, except very near to the band edges. The shape of the bands, and their temperature dependence, must be known in order to calculate the intrinsic reaction constant at high temperatures. Even low-temperature properties for n-type material with $n > 10^{14}$ will have interpretations much different from those deduced from parabolic band structures. These modified properties include the electron mobilities, lifetimes, absorption coefficients, responsivities, and noise currents.

2.2 DISLOCATIONS IN HgCdTe

A large body of experimental evidence has established that dislocations adversely affect the device performance of photovoltaic detectors. It is generally agreed that the presence of dislocations reduces the minority carrier lifetime^{1,2} and diffusion length^{3,4} of the semiconductor, increases the leakage current⁵, and reduces the resistance⁶ and the open circuit voltage⁷ of the detector diodes. Johnson *et al.*⁶ have very recently summarized the effect of dislocations on the electrical and optical properties of HgCdTe (MCT), and Shin *et al.*² have explored techniques for reducing dislocation densities in MCT grown heteroepitaxially on GaAs and Si using minority carrier density as a diagnostic tool.

Dislocations are thought to affect the properties of MCT by acting as scattering and recombination centers. To account for this activity, it is necessary to explain how dislocations can give rise to the electric fields that affect carrier dynamics. Such electric fields can be associated with the band bending arising from gap states in dislocation cores, and from the strain fields in the dislocation's vicinity. We are considering both these effects for the present study, because it appears that both may be needed to account for the observations, and for the development of effective design rules for MCT photovoltaic detector arrays.

Dislocation cores must certainly give rise to bound states in the semiconductor band gap, and it is believed that those dislocation cores terminating on a line of Te atoms in n-type MCT may be inverted, and surrounded by a depleted space-charge region. Analysis of the fields in this region using the depletion approximation predicts depletion region radii of the order of, or even smaller than, the Debye length. A more accurate analysis using a somewhat less crude approximation (see Appendix B) predicts that small but still noticeable fields persist to larger radii, resulting, for example, in a radius of the field region of a dislocation in $n = 10^{14} \text{ cm}^{-3}$ MCT of the order of 5 μm . Minority carriers within this radius will have their lifetimes shortened. While

this can give rise to significant effects, it does not appear adequate to account for the observed phenomena.

The effect of strain on the current-voltage relation of InSb and MCT has been investigated^{5,8} and the observations have been interpreted in terms of the piezoelectric fields associated with the strain. Strain scattering by point defects in piezoelectric semiconductors has been analyzed by Fedders.⁹ We are carrying out a similar analysis (see Appendix C) for piezoelectric-induced effects caused by the strain field of dislocations. Some aspects of this interaction can be understood from symmetry considerations. The piezoelectric tensor of the sphalerite structure couples only shear strains to the crystal's electric polarization. The strain field of a long straight dislocation and the electric polarization that it induces are planar, that is to say, independent of the coordinate along the dislocation direction. The piezoelectric field that scatters the carriers is generated by the bound charge density associated with the divergence of the polarization. The polarization has nonzero divergence only if the strain displacement (and Burger's vector) has a component along the dislocation axis. Therefore, straight edge dislocations produce no scattering field, but screw and mixed dislocations do. Kinks, jogs, and nonparallel dislocations are also expected to generate piezoelectric fields that can act as scattering and recombination centers. For a quantitative analysis we need the piezoelectric coupling constant¹⁰ of MCT and structural information about dislocation types. This work is in progress.

3. PHOTONIC MATERIALS

For research on the wide-gap II-VI compound, ZnSe was chosen as the prototype and much of the effort has been in establishing the groundwork for doing the relaxed defect calculations and the gradient correction, as discussed in the introduction. The cohesive energy and bond length of ZnSe have been calculated and are found in good agreement with experiment. We have begun the calculation of the native defect formation energies. Cation and anion vacancies, antisites, and two classes of cation and anion interstitials are being included.

4. WORK PLANNED

In the next quarter, we will continue work to improve the value of the intrinsic reaction constant that is necessary to calculate the ionized defect concentration in HgCdTe. We will calculate the relaxed neutral native defect energies in HgCdTe and in ZnSe. We will examine eight defects: the cation and anion vacancies, the cation and anion antisites, and the cation and anion at two different interstitial sites. Upon completion of these calculations we will redo the ionized defect density calculations in HgCdTe, and make our first predictions of neutral native defect densities in ZnSe.

REFERENCES

1. R.K. Ahrenkiel, M.M. Al-Jassim, B. Keyes, D. Dunleavy, K.M. Jones, S.M. Vernon, and T. M. Dixon, *J. Electrochem. Soc.* **137**, 996 (1990).
2. S.H. Shin, J.M. Arias, D.D. Edwall, M. Zandian, J.G. Pasko, and R.E. DeWames, *J. Vac. Sci. Technol.* **B10**, 1492 (1992).
3. Y.K. Grutogolov, V.P. Gorshov, S.A. Bondar, L.V. Lebedeva, and S.S. Strel'chenko, *Sov. Phys. Semicond.* **14**, 756 (1980).
4. M. Yamaguchi, A. Yamamoto, and Y. Itoh, *J. Appl. Phys.* **59**, 1751 (1986).
5. S. Maniv, M. Shamai, and Y. Sinai, *J. Appl. Phys.* **62**, 4916 (1987).
6. S.M. Johnson, D.R. Rhiger, J.P. Rosbeck, J.M. Peterson, S.M. Tailor, and M.E. Boyd, *J. Vac. Sci. Technol.* **B10**, 1499 (1992).
7. J.C. Zolper and A.M. Barnett, *Trans. IEEE.* **ED 37**, 478 (1990).
8. E. Weiss and N. Mainzer, *J. Vac. Sci. Technol.* **A7**, 391 (1989).
9. P.A. Fedders, *J. Appl. Phys.* **54**, 1804 (1983).
10. Santa Barbara Research Center, "Physics of Failure of IRFPAs," Final Report to Naval Research Laboratory (December 1991).

Appendix A

Hg_{0.8}Cd_{0.2}Te NATIVE DEFECTS: DENSITIES AND DOPANT PROPERTIES

$Hg_{0.8}Cd_{0.2}Te$ Native Defects: Densities and Dopant Properties

M.A. Berding, M. van Schilfgaarde, and A. Sher

SRI International, Menlo Park, CA 94025

We examine the native defect equilibrium in $HgCdTe$, including cation and anion vacancies, interstitials, and antisites in the analysis. A gradient correction to the local density functional has been added to the defect formation enthalpies calculated within the local density approximation, and preliminary predictions of the dominant ionization states are made. Temperature-dependent defect formation entropies and the temperature dependence of the preexponentials are incorporated into the calculation of the defect densities. Degenerate Fermi-Dirac statistics are used for the electronic equilibration, and the intrinsic reaction constant as a function of composition and temperature is calculated. We theoretically substantiate the doubly ionized mercury vacancy as the dominant defect in $HgCdTe$, and expect the doubly ionized mercury vacancy densities to be comparable in $HgZnTe$. We predict that tellurium antisites are donors and will be present for some annealing conditions in sufficient quantities to be measured and possibly to affect device performance.

I. INTRODUCTION

The importance of native defects in HgCdTe is undisputed, with the dominant defect believed to be the double acceptor Hg vacancy.¹ The evidence for these defects is largely indirect and depends on their being ionized for observation. Neutral defects and compensating defects are more difficult to measure, and neither their densities nor even their presence is well established.

Our goal is to identify the important native defects in HgCdTe as a function of temperature and mercury pressure. Predictions of the absolute defect concentrations are difficult because of the accuracy required for reaction enthalpies and entropies that enter in exponentials. Our calculations although using a state-of-the-art method, are subject to a number of limitations, such as the supercell approximation that is used to calculate defect formation enthalpies. Despite these limitations, for which error bars can be estimated, we find good agreement with experiment for the defect densities in narrow-gap HgCdTe. While there are some fitted parameters in the theory — for example, the temperature variation of the band gap — none have been chosen to fit the measured defect densities we are predicting. Thus, deviations must be ascribed to deficiencies in our approximations or to physical mechanisms that have not yet been incorporated.

In our previous work, we used the linearized muffin-tin orbital (LMTO) method within the atomic spheres approximation (ASA),² and later the full-potential (FP) Harris Foulkes approximation.³ The ASA substitutes a spheridized density for the true Hohenberg-Kohn density functional in the local density approximation. While the ASA is computationally fast, it cannot reliably predict atomic forces, and therefore lattice relaxations. Because of the elimination of the ASA shape approximation, in the FP calculations we have predicted the breathing mode relaxations about the defect sites. Using the resulting defect formation enthalpies, in Ref. 3 we predicted ratios of neutral native defects. In the present paper we have made several important improvements to this previous work: (1)

a gradient correction to the local density functional⁴ has been included, which we find has a significant impact on the defect formation enthalpies; (2) absolute defect densities are predicted; (3) the reaction constant for electron-hole pair production as a function of temperature and cadmium composition for degenerate Fermi-Dirac statistics is predicted; and (4) the primary ionization states of the native defects have been tentatively identified and incorporated into the defect equilibrium.

The problem of predicting the defect concentrations is complicated by the fact that we are dealing with an alloy. The defect formation energies were calculated for HgTe, the primary component of the pseudobinary alloys HgCdTe and HgZnTe. Using a tight-binding model we have shown⁵ that the vacancy formation energy has a nonlinear dependence on the constituents in the near alloy environment, with the nonlinearity being most dramatic for the removal of the common-lattice atom (i.e., tellurium for HgCdTe and HgZnTe). The variation of the mercury vacancy formation energy, while less dramatic because the first-nearest neighbors are always tellurium, is as much as ~ 0.1 eV (depending on the constituents in the second-neighbor shell). We have not yet incorporated this level of detail into our first-principles calculations. Additionally, we have not included cadmium- or zinc-based defects (such as the cadmium antisite); because HgTe is the dominant constituent for compositions of technological importance, we believe this exclusion is justified. The alloy effects have been included in the present calculations via the composition dependence of the bandgap which, because of its temperature dependence, has been extracted from experiment and the shape of the conduction and valence bands.

II. REACTION ENTHALPIES

We consider the following native defects: mercury vacancy V_{Hg} , tellurium vacancy V_{Te} , mercury antisite Hg_{Te} , tellurium antisite Te_{Hg} , mercury interstitial Hg_i , and tellurium interstitial Te_i . A couple of corrections have been added to the reaction enthalpies calcu-

lated within the Harris-Foulkes approximation to the FP-LMTO. First, the ASA is used to determine the ionization state of the defect — that is, whether it is a donor or acceptor. We have not yet determined the ionization energies of the defect, but we do indicate whether the state appears to be “deep” or “shallow.” We assume that only the shallow states are electrically active. Because we have not yet determined the ionization energies, we will for the present assume that they are zero for the shallow states — that is, that the donor and acceptor levels lie close to the conduction and valence band edges, respectively. We assume that the deep states are not electrically active. This approximation is likely to be good because, at high temperatures where the defect concentrations are equilibrated, carrier concentrations are high enough so that free carrier screening may effectively reduce the shallow-state activation energies. Details of the calculational method used to determine the ionization states of the various defects will be reported elsewhere.

The second correction to results involves the incorporation of a gradient correction to the local density functional. This correction has not yet been implemented in the FP-LMTO, and thus was done within the ASA. We expect that the FP gradient correction will be nearly equal to that from the ASA, because the density gradient is predominantly radial, the nonspherical components eliminated in the ASA being small. In Table I we summarize the formation energies including the gradient correction for the neutral defect reactions in Eqs. (1)–(6) below. Also shown are the cohesive energies of the constituent compounds HgTe, CdTe, and ZnTe from a gradient-corrected self-consistent FP calculation; one can see that the agreement with experiments is quite good. The tentative identification of defect ionization states is also given in Table I.

III. DEFECT CONCENTRATIONS

Defect concentrations are determined using a quasi-chemical analysis of the defect formation reactions.⁶ We consider the following defect reactions



where we have chosen the HgTe unit cell and free atomic mercury, Hg_I , as the reference states. Other reactions of interest can be obtained by taking linear combinations of these equations. For example the neutral Schottky defect reaction is obtained by adding Eqs. (1) and (2) to obtain



or, as it is more commonly written,



The concentrations of the defects in Eqs. (1)–(6) can be obtained from the evaluation of the corresponding reaction constants:

$$K_{V_{\text{Hg}}} = [V_{\text{Hg}}]p_{\text{Hg}} \quad (9)$$

$$K_{V_{\text{Te}}} = [V_{\text{Te}}]/p_{\text{Hg}} \quad (10)$$

$$K_{\text{Hg}_{\text{Te}}} = [\text{Hg}_{\text{Te}}]/p_{\text{Hg}}^2 \quad (11)$$

$$K_{\text{Te}_{\text{Hg}}} = [\text{Te}_{\text{Hg}}]p_{\text{Hg}}^2 \quad (12)$$

$$K_{Hg_I} = [Hg_I]/p_{Hg} \quad (13)$$

$$K_{Te_I} = [Te_I]p_{Hg}. \quad (14)$$

In these expressions, p_{Hg} is the mercury pressure in atmospheres and square brackets refer to concentrations per cubic centimeter. The evaluation of these reaction constants was discussed in our previous paper³ as well as in many standard texts.⁷ In the present calculations, we have used the formation energies from Table I and temperature-dependent entropies given in Ref. 3.

Ionized defect concentrations can be determined from the concentration of neutral defects from

$$[D'] = (g_{D\cdot}/g_{D^*}) \exp((E_{D\cdot} - E_F)/k_B T) [D^*] \quad (15)$$

for donors and

$$[A'] = (g_{A\cdot}/g_{A^*}) \exp((E_F - E_{A\cdot})/k_B T) [A^*] \quad (16)$$

for acceptors. The dot and prime superscripts correspond to a positively and negatively charged species, respectively; g_X is the degeneracy of the state X ; $E_{D\cdot}$ and $E_{A\cdot}$ are the positions of the first ionization levels for the donor and acceptor, respectively; in the one-electron picture, E_F is the Fermi energy, k_B is Boltzmann's constant, and T is the temperature in Kelvin. Similar expressions are obtained for the second ionization state.

In addition to the above equations for the determination of the native defect populations, we have the reaction for the generation of electron-hole pairs



The corresponding reaction constant is

$$K_{pn} = [h][e'] = pn \quad (18)$$

where $p = [h]$ and $n = [e']$, as in the usual notation.

In general, K_{pn} depends on the structure of the conduction and valence bands, the band gap energy, the Fermi energy, and the temperature variation of these quantities. Several limits are often encountered in the evaluation of K_{pn} . First, when the conduction and valence bands are parabolic, although not necessarily isotropic, $E \sim k^2$, and the reaction constant can be written in terms of the Fermi-Dirac integrals as

$$K_{pn} = 4 \left(\frac{2\pi k_B T}{h^2} \right)^3 (m_h m_e)^{3/2} F_{1/2} \left(\frac{E_F - E_c}{k_B T} \right) F_{1/2} \left(\frac{E_v - E_F}{k_B T} \right) \quad (19)$$

where $F_{1/2}$ is the Fermi-Dirac function; E_c , E_v , and E_F are the conduction-band, valence-band, and Fermi energy, respectively; m_h and m_e are the hole and electron density-of-states effective masses, respectively; and h is Planck's constant. In the nondegenerate limit, this reduces to the familiar expression

$$K_{pn} = 4 \left(\frac{2\pi k_B T}{h^2} \right)^3 (m_h m_e)^{3/2} \exp \left(\frac{E_v - E_c}{k_B T} \right) \quad (20)$$

which is independent of the Fermi energy. For the general degenerate case, which will apply even at moderate temperatures for narrow-gap HgCdTe, K_{pn} will depend on E_F and therefore in general will not be independent of the presence of extrinsic carriers. Additionally, the assumption of parabolic bands may be poor for the narrow-gap materials, where the dispersion near the conduction band edge is rather more linear than parabolic,⁸ i.e., $E = \alpha k$. This case obtains with the Fermi-Dirac integral function of order 2 and

$$K_{pn} = 2 \left(\frac{2\pi k_B T m_h}{h^2} \right)^{3/2} \frac{2}{\pi^2} \left(\frac{k_B T}{\alpha} \right)^3 F_2 \left(\frac{E_F - E_c}{k_B T} \right) F_{1/2} \left(\frac{E_v - E_F}{k_B T} \right). \quad (21)$$

In the present program, we have used Eq. (21) to evaluate K_{pn} , with $m_h = 0.43$,

$$E_g(x, T) = E_c - E_v = -0.313 + 1.787x + 0.444x^2 - 1.237x^3 + 0.932x^4 \\ + (0.667 - 1.714x + 0.760x^2)T/1000 \quad (22)$$

taken from Ref. 9, and α chosen to yield good agreement with experimental values of the intrinsic carrier concentrations.¹⁰

The calculation of the intrinsic reaction constant for narrow-gap HgZnTe is more difficult to evaluate, given the more limited data base for evaluation of the high-temperature band gap, effective masses, and intrinsic carrier concentration. From the zero-temperature band structures, the valence-band effective masses are found to be comparable for HgCdTe and HgZnTe with equal band gaps, while the conduction-band effective mass for HgZnTe is slightly larger than for HgCdTe.¹¹ Overall, though, we expect K_{pn} for the two materials to be comparable.

To calculate the native defect concentrations at a given temperature and mercury pressure, we have to determine the Fermi energy which satisfies the neutrality condition

$$2 \sum_i [D_i^-] + \sum_i [D_i] + [h] = 2 \sum_i [A_i^{''}] + \sum_i [A_i'] + [e']. \quad (23)$$

The concentrations of neutral defects which are independent of the Fermi energy can be solved for directly for a given p_{Hg} , and T .

IV. RESULTS

The low-temperature (77 K) hole concentrations as a function of mercury pressure for various equilibration temperatures are shown in Figure 1 for $x = 0.2$ Hg_xCd_{1-x}Te. Shown for comparison are the experimental data from Vydyanath.¹ In the calculations, we allowed both atomic and electronic equilibrations at the high temperature at which the annealing takes place; we then assume the total defect concentrations are frozen-in upon quenching,

and that at 77 K only the electronic equilibrium is reestablished. In agreement with Vydyanath,¹ we conclude that the mercury vacancy is the dominant defect in HgCdTe, and it behaves as a double acceptor. We have not yet determined the activation energy for the vacancy. We find the tellurium antisite, which is a donor, is also an important defect. In Figure 2 we show a breakdown of the concentrations of various defects at 500°C as a function of mercury pressure. At low mercury pressures, the tellurium antisite density becomes comparable to that of the mercury vacancy and results in a high degree of compensation; it is the compensating tellurium antisite donors that are responsible for the roll-off on the low-pressure side of the concentration curves in Fig. 1.

The remaining discrepancies between our results and experiment can be attributed to a number of factors. First, we have calculated the formation energies for HgTe and applied them directly to HgCdTe, with the alloy taken into account in the calculation of the reaction constant for electron-hole pairs, and in the assumption that the defect ionization levels are at the band edges. Although this should be a reasonable approximation, we have shown that the vacancy formation energies are sensitive to the near-neighbor environment.⁵ The removal of this approximation will lead to a raising of the vacancy formation energy by as much as ~ 0.1 eV and, from examination of Fig. 1, will yield better agreement with experiment. Next, we have not taken into account the nonradial relaxation about the vacancy site and its effect on both the formation energy and entropy, nor have we yet included the effect of the entropy of local-mode softening of the ionized vacancy relative to the neutral vacancy. Additionally, the correct ionization energy must be incorporated into the calculation. Finally, we have used a band structure in calculating the reaction constant for electron-hole pairs which yields agreement with the intrinsic carrier concentrations and band gap at $T < 400$ K; the band structure at higher temperatures is speculative, and we need further experiments or theory to confirm its validity.

At the annealing temperature, the material is intrinsic and all of the native defects are

nearly completely ionized. While the total numbers of defects are frozen-in upon quenching from high temperature, the ratio of ionized to nonionized defects does change. At 77 K the material is extrinsic and, for material annealed at high temperatures ($T > 400^\circ\text{C}$), is dominated by the acceptor level of the mercury vacancy. Consequently, upon quenching, the ratio of ionized to nonionized defects decreases for acceptor defects and increases for donor defects.

Defect densities present after a low temperature ($\sim 250^\circ\text{C}$) annealing under mercury-saturated conditions are of technological interest. Our predictions for defect concentration as a function of $1/T$ for mercury pressures corresponding to mercury saturated conditions are shown in Figure 3. At $T < 300^\circ\text{C}$, a mercury-saturated annealing step is effective in reducing the vacancy concentration to less than 10^{15}cm^{-3} . Because the density of tellurium antisites varies as P_{Hg}^{-2} , compared to P_{Hg} for the mercury vacancy, the antisites are most important on the tellurium-rich side of the stability region, and thus are less important for these mercury-saturated annealing.

While the mercury vacancy and tellurium antisite are the primary defects that will affect the electrical activity in $\text{Hg}_{0.8}\text{Cd}_{0.2}\text{Te}$, several other defects are of interest because of their role in diffusion, for example the mercury and tellurium interstitials. In Figure 2, we see that the densities of mercury antisites and mercury interstitials are less than 10^{10}cm^{-3} , while the densities of tellurium vacancies and interstitials are completely negligible. The defect formation energies used for the calculation of the interstitial densities were from our ASA calculations without lattice relaxations, and therefore carry a larger uncertainty than the antisite and vacancy formation energies. We expect that improvement of the defect total-energy calculations will result in a potentially significant lowering of the formation energy, and consequently an increase in the interstitial defect concentrations. Even so, it is doubtful that we will find tellurium interstitials at densities large enough to account for the tellurium diffusion, which was believed to be via the tellurium interstitials.

While the tellurium antisites are donors and are predicted to be present in significant densities in HgCdTe, we do not predict that equilibrated tellurium antisites are responsible for the experimentally observed p-to-n conversion. Even if such a p-to-n conversion were to occur as a consequence of refinements in our calculations, the conversion would occur on the tellurium-rich side of the stability region. Because antisites are likely to be immobile, relatively high densities of tellurium antisites introduced at high temperatures during growth may persist through low-temperature annealings undertaken to remove mercury vacancies. In this case the tellurium antisites could be responsible for the p-to-n conversion. A careful correlation of the n-type character with the high-temperature preparation conditions would help to confirm or negate this possibility.

Because of the similar magnitude for the electron and hole effective masses in narrow-gap HgCdTe and HgZnTe, we expect that the intrinsic reaction constants will be similar in the two materials. In addition, the mercury vacancy formation energy will be similar in the two materials for compositions low in cadmium or zinc, and therefore we expect the defect concentrations to be similar in the low- x materials with comparable bandgaps. The tellurium antisite was found to be strained in the HgTe lattice,^{2,3} and produced a compressive strain in the surrounding lattice. Because of the shorter bond lengths in the HgZnTe alloy, the strain associated with the tellurium antisite is larger than in HgCdTe with a comparable bandgap; consequently the formation energy is expected to be larger in HgZnTe. Thus, we expect the tellurium antisites to be less important in HgZnTe than in HgCdTe. If the tellurium antisite is responsible for the residual n-type character in low-temperature annealed material, lower n-type carrier concentrations will be realizable in HgZnTe.

V. CONCLUSIONS

We have calculated the low-temperature hole concentration as a function of anneal-

ing temperature and pressure for HgCdTe. We find good agreement with the fit to the experimental data. Remaining discrepancies can be attributed to relaxation and finite ionization energies in the vacancy formation energies, and uncertainties in K_p at high temperatures. We conclude, in agreement with experiment, that the dominant defect is the doubly ionized mercury vacancy. We do not make any conclusions about the presence of the singly ionized Hg vacancy; we will examine the activation energies for both the singly and doubly ionized states in future work. We find that tellurium antisites are donors and are present in significant densities for low mercury pressures at temperatures above 350 K. At lower temperatures and high mercury pressures, at which annealing typically takes place, tellurium antisite equilibrium densities are negligible. However if their density remains at levels corresponding to high temperature because their low temperature diffusivities are low, then such antisites could affect mobilities and even be the "residual donor." None of the other native defects are present in sufficient quantity to influence device characteristics.

ACKNOWLEDGMENTS This work has been supported by DARPA Contract MDA972-92-C-0053, NASA Contract NAS1-18226, and ONR contract N00014-89-K-132. Computational support provided by the Numerical Aerodynamical Simulation computing facility at NASA Ames Research Center.

REFERENCES

1. H.R. Vydyanath, *J. Electrochem. Soc.* **128**, 2609 (1981).
2. M.A. Berding, M. van Schilfgaarde, A.T. Paxton, and A. Sher, *J. Vac. Sci. Technol. A* **8**, 1103 (1990).
3. M.A. Berding, M. van Schilfgaarde, and A. Sher, *J. Vac. Sci. Technol. B* **10**, 1471 (1992).
4. D. Lengreth and D. Mehl, *Phys. Rev. B* **28**, 1809 (1983).
5. M.A. Berding, A. Sher, and A.-B. Chen, *J. Appl. Phys.* **68**, 5064 (1990); *J. Vac. Sci. Technol. A*, **5**, 3009 (1987).
6. F.A. Kroger and H.J.Vink, in *Solid State Physics Vol. 9*, edited by F. Seitz and D. Turnbull (Academic Press, New York 1956), p. 307.
7. For example, see F. Reif, *Fundamentals of Statistical and Thermal Physics* (McGraw-Hill, New York, 1965).
8. A.-B. Chen, M. van Schilfgaarde, and A. Sher, this conference.
9. *Properties of Mercury Cadmium Telluride*, edited by J. Brice and P. Capper (INSPEC, New York, 1987), p. 105.
10. *ibid.*, p. 110.
11. M.A. Berding, S. Krishnamurthy, A. Sher, and A.-B. Chen, *J. Vac. Sci. Technol. A* **5**, 3014 (1987).

FIGURE CAPTIONS

FIGURE 1. Hole concentrations at 77 K as a function of mercury pressure for material annealed at high temperatures. Experimental data were taken from Vydyanath¹. Theory is shown as solid lines for pressures within the stability region at a given temperature.

FIGURE 2. Predicted defect densities at 500 K as a function of mercury pressure

FIGURE 3. Defect densities as a function of temperature for mercury-saturated annealing conditions

TABLE I. Formation energies and ionization states of the native point defects. Formation energies refer to the neutral defect reactions in Eqs. (1)–(6) in text. See text for discussion of *shallow* and *deep*. Experimental cohesive energies are shown in parentheses.

Defect	Formation energy (eV)	Ionization state
V_{Hg}	1.93	shallow acceptor
V_{Te}	2.39	donor
Te_{Hg}	2.68	shallow donor
Hg_{Te}	0.75	deep acceptor
Te_I	4.47	shallow donor
Hg_I	1.75	shallow donor
 ZnTe	 4.66 (4.8)	
CdTe	4.17 (4.4)	
HgTe	3.37 (3.3)	

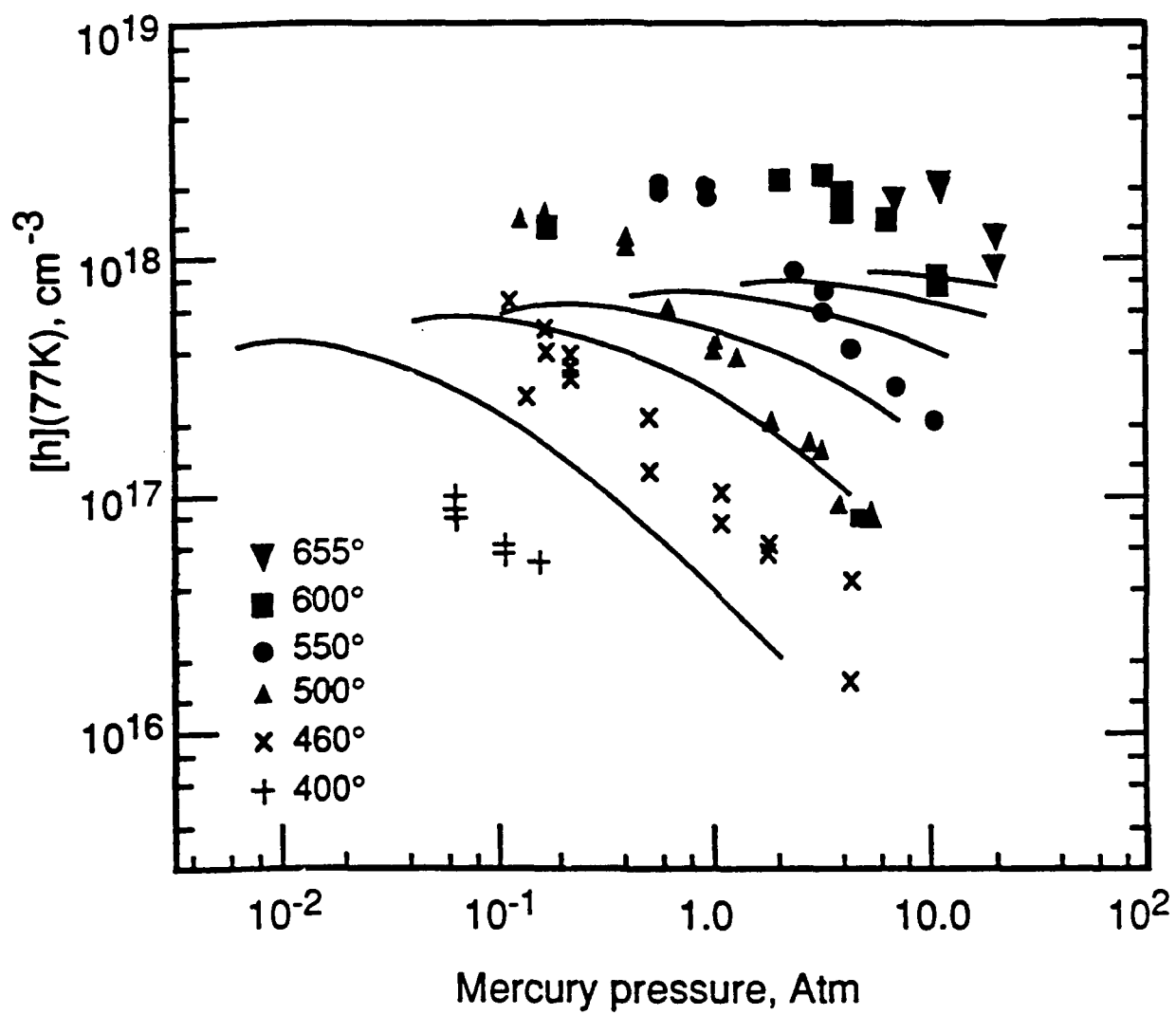


Figure 1

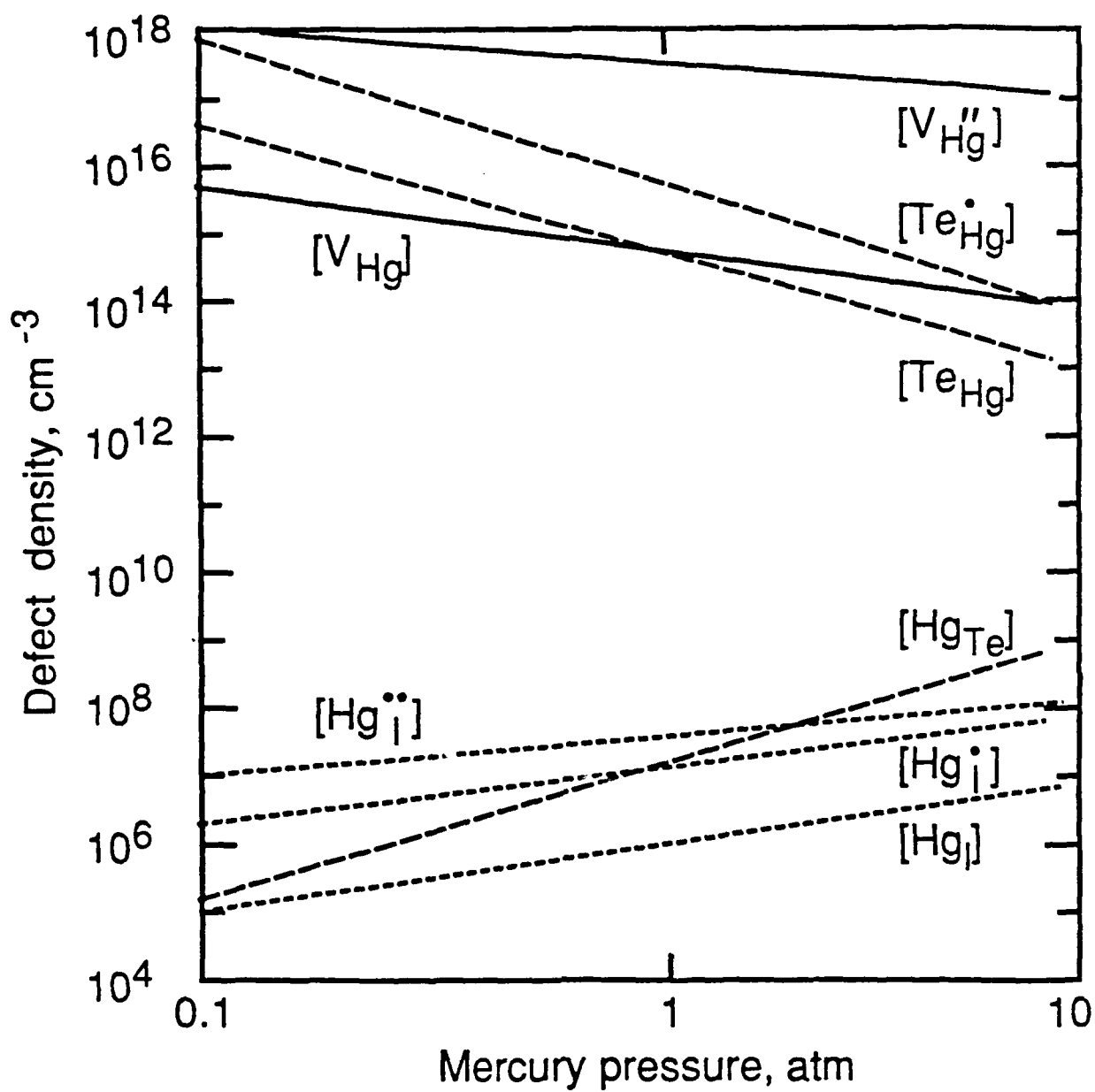


Figure 2

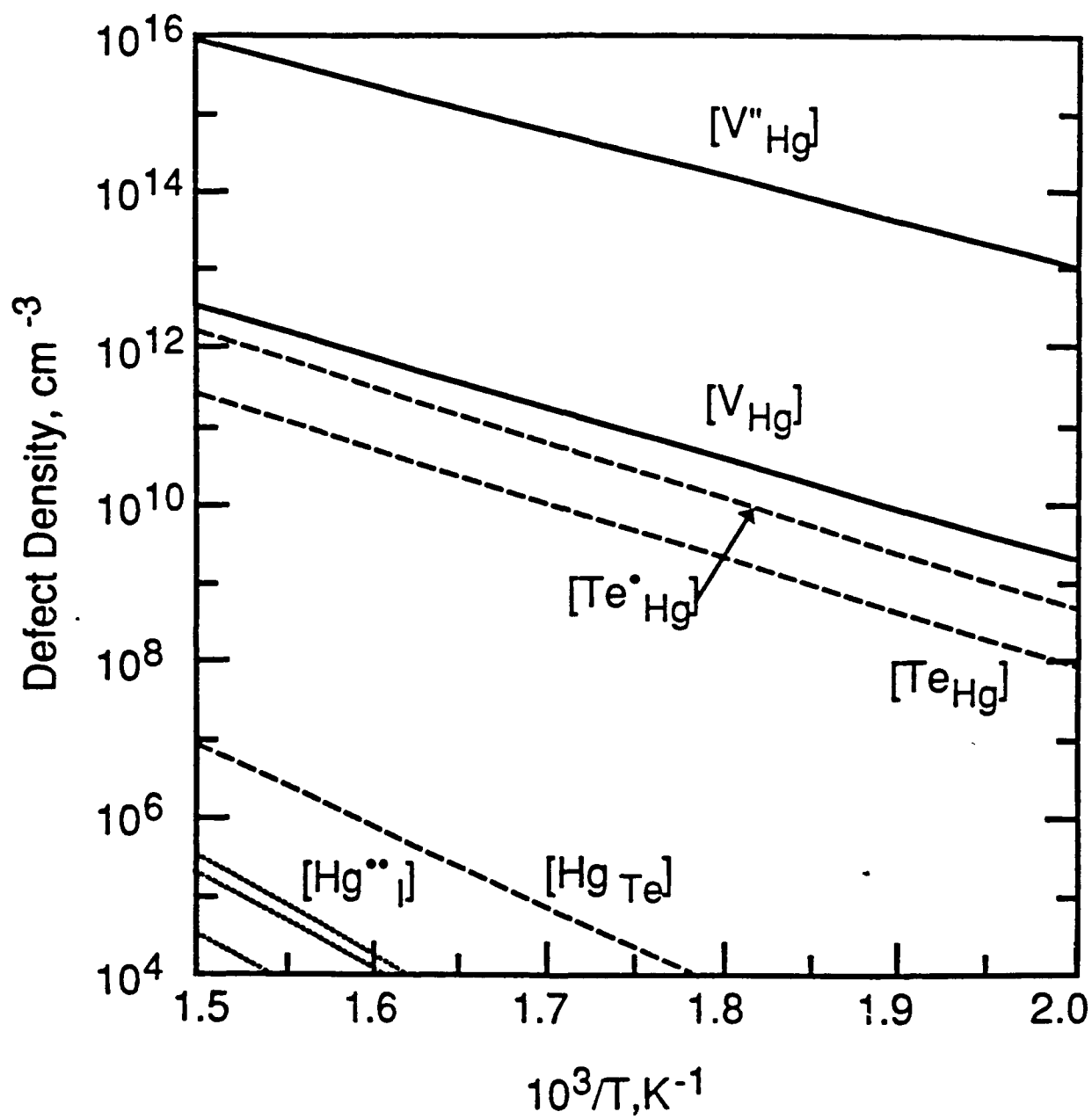


Figure 3

Appendix B
DISLOCATION SPACE CHARGE

DISLOCATION SPACE CHARGE

Represent the dislocation core by a cylindrical charge density $-p$ in a cylinder of radius a in n-type material with donor density n . The potential distribution in the depletion approximation is given by the Poisson equation with charge density ρ

$$\begin{aligned}\rho &= (-p + n)e & r < a \\ &= ne & a < r < R \\ &= 0 & R < r\end{aligned}$$

where R is the depletion radius, related to a by the charge neutrality requirement $pa^2 = nR^2$. By integrating the Poisson equation we find for the potential

$$\phi(r) = \phi(a) + \frac{en}{2\epsilon} \left[R^2 \ln \frac{r}{a} - \frac{1}{2} (r^2 - a^2) \right]$$

and we take the potential in the bulk ($r \geq R$) as reference; we can evaluate the potential at the core radius

$$\phi(a) = \frac{en}{2\epsilon} \left[\frac{1}{2} (R^2 - a^2) - R^2 \ln \frac{R}{a} \right].$$

In MCT a reasonable value of the dislocation core radius is 5×10^{-8} cm and a potential relative to the bulk at the core radius of 0.1 V. A table of depletion radius versus doping level for these values is

n, cm^{-3}	10^{13}	3×10^{13}	10^{14}	3×10^{14}	10^{15}	3×10^{15}	10^{16}	3×10^{16}
R, cm	1.70×10^{-4}	1.01×10^{-4}	5.81×10^{-5}	3.49×10^{-5}	2.01×10^{-5}	1.22×10^{-5}	7.05×10^{-6}	4.32×10^{-6}

These radii are close enough to the Debye length to make the depletion approximation questionable. The exact space charge equation is

$$\frac{1}{r} \frac{d}{dr} r \frac{d\phi}{dr} = \frac{2}{L^2} [\sinh(\phi - \phi_F) = \sinh \phi_F]$$

where

$$\phi = \frac{e\phi}{kT}, L^2 = \frac{\epsilon kT}{e^2 n_i}, \phi_F = \frac{E_F - E_i}{kT} = \sinh^{-1} \frac{N_D - N_A}{n_i}$$

For ϕ small this is

$$\frac{1}{r} \frac{d}{dr} r \frac{d\phi}{dr} \equiv \left(\frac{2}{L_D^2} \cosh \phi_F \right) \phi = \frac{2}{L_D^2} \phi$$

with the extrinsic Debye length $L_D^2 = \frac{L^2}{\cosh \phi_F} \equiv \frac{\epsilon kT}{e^2 N_D} = \frac{2.77 \times 10^5}{N_D}$, N_D in cm^{-3}

Then with $x = \frac{r}{L_D}$ we have $\frac{1}{x} \frac{d}{dx} x \frac{d\phi}{dx} = \phi$, the zero-order modified Bessel equation. The solution of interest is the decreasing Hankel function $K_0(x)$.

The depletion approximation should be valid for $r < R = L_D$. This does not leave much room since R and L_D are comparable. One way to proceed is to let $\phi = CK_0(x)$ and to evaluate C from $\phi(a)$ at $x = a/L_D$. Then we can determine the effective scattering radius of the dislocation as the radius at which the field is reduced to a small enough value, say 10^{-2} V/cm. The space charge field is given by

$$E = \frac{d\phi}{dr} = \frac{kT}{e} \frac{d\phi}{dr} = \frac{kT}{eL_D} \frac{d\phi}{dx} = \sqrt{\frac{n_D kT}{\epsilon}} CK_1(x) = 4.75 \times 10^{-5} \sqrt{N_D} CK_1(x).$$

For the core radius of 5×10^{-8} cm and core edge potential of 0.1 V, and a donor concentration of 10^{14} cm^{-3} we find $L_D = 5.26 \times 10^{-5}$ cm, $a/L_D = 9.5 \times 10^{-4}$.

For x small, $K_0(x) \equiv \ln \frac{2}{\gamma x} = 0.116 - \ln x$, $K_0\left(\frac{a}{L_D}\right) = 0.116 + 6.96 = \frac{\phi(A)}{C}$.

Since $\phi(a) = \frac{kT}{e} \phi(a) = 0.025 \phi(a) = 0.1$ this gives $C = 0.56$, and

$$E = 4.75 \times 10^{-5} \times 10^7 \times 0.56 K_1(x) = 266 K_1(x).$$

For x large, $E = 266 \sqrt{\frac{\pi}{2x}} e^{-x} = 333 \frac{e^{-x}}{\sqrt{x}}$.

To reduce E to 10^{-2} V/cm we need $e^{-x}/\sqrt{x} = 3 \times 10^{-5}$, $x = 9.3$, $r = 4.9 \times 10^{-4}$ cm.

Appendix C
PIEZOELECTRIC FIELD OF A STRAIGHT DISLOCATION

PIEZOELECTRIC FIELD OF A STRAIGHT DISLOCATION

The polarization produced by a strain u_{jk} is given by $P_i = -e_{ijk}u_{jk}$, where e_{ijk} is the ijk component of the piezoelectric tensor (piezoelectric coupling constant) and where $u_{jk} = \frac{1}{2} \left(\frac{\partial u_i}{\partial r_j} + \frac{\partial u_j}{\partial r_i} \right)$, with u_k the k -component of the stress-induced distortion.

In the sphalerite structure the only nonzero component of the piezoelectric tensor is e_{14} if i, j , and k are all different. Since there is no free charge in an insulating crystal, the displacement is solenoidal, $\text{div} D = 0$, and the potential is given by $\nabla^2 \phi = -4\pi \rho(r)$, with an effective bound charge density $\rho(r) = \frac{1}{\epsilon} \frac{\partial}{\partial x_i} [e_{ijk} u_{jk}(r)]$.

If we take the z -axis along the direction of a straight dislocation, all the strains are functions of x and y only. For an edge dislocation* the only shear strain is

$$u_{xy} = \frac{bx(y^2 - x^2)}{4\pi(1 - \nu)(x^2 + y^2)^2}$$

where b is Burger's vector and ν is Poisson's ratio. For a screw dislocation along the z -axis with $b = bz$ the shear strains are

$$u_{xz} = \frac{by}{4\pi(x^2 + y^2)}, \quad u_{yz} = \frac{bx}{4\pi(x^2 + y^2)}.$$

It is apparent that no bound charge density, and hence no piezoelectric field, is associated with a pure edge dislocation. The bound charge density associated with a pure screw dislocation is

$$\rho = \frac{be_{14}}{4\pi} \left(\frac{\partial}{\partial x} \frac{x}{x^2 + y^2} - \frac{\partial}{\partial y} \frac{y}{x^2 + y^2} \right) = \frac{be_{14}}{2\pi} \frac{y^2 - x^2}{(x^2 + y^2)^2}$$

* See, for example, D. Hull and D.J. Bacon, "Introduction to Dislocations," 3rd ed. Pergamon 1984.